

# Baseband Characterization of Additive White Symmetric $\alpha$ -Stable Noise

Ahmed Mahmood, Mandar Chitre and Marc A. Armand

Department of Electrical and Computer Engineering, National University of Singapore, Singapore 117576

e-mail: {ahmed.mahmood, mandar, eleama}@nus.edu.sg

**Abstract**—The performance of conventional digital communication schemes in the presence of additive white Gaussian noise (AWGN) has been widely studied and optimized. The efficiency of these systems, however, is severely hampered if the channel noise is impulsive. Impulsive noise is non-Gaussian in nature and is modeled well by random processes based on heavy-tailed symmetric  $\alpha$ -stable (S $\alpha$ S) distributions. If the noise samples are identical and mutually independent, the additive white S $\alpha$ S noise (AWS $\alpha$ SN) model is used to simulate the channel. As performance is conventionally analyzed at the baseband level, we investigate characteristics of complex baseband noise derived from passband AWS $\alpha$ SN. The baseband noise samples are shown to be mutually independent with identical distribution. The bivariate distribution of each complex noise sample takes on a star-like geometrical configuration. We also investigate the baseband scale parameter as a function of the noise impulsiveness and system parameters.

## I. INTRODUCTION

The motivation of using heavy-tailed symmetric  $\alpha$ -stable (S $\alpha$ S) models to emulate impulsive noise stems from the generalized central limit theorem (GCLT) [1]–[3]. The GCLT states that the sum of  $N$  independent and identically distributed (IID) random variables converges to that of a *stable* random variable as  $N \rightarrow \infty$ . This convergence phenomenon is uniquely attributed to stable distributions and is termed as the *stability property*. The relatively well-known class of Gaussian distributions also share the aforementioned property and thus are members of the stable family. With the exception of the Gaussian case, all stable distributions are heavy-tailed. This makes non-Gaussian S $\alpha$ S distributions suitable for modeling datasets with a large number of outliers [2], [3].

A stable random variable is S $\alpha$ S if its probability density function (pdf) is symmetric about zero. The zero-mean Gaussian distribution is a member of the S $\alpha$ S family. The *characteristic exponent* ‘ $\alpha$ ’ quantizes the tail-heaviness of any stable distribution and lies within  $(0, 2]$ . For  $\alpha = 2$  and  $\alpha = 1$  the distributions are Gaussian and Cauchy, respectively. As  $\alpha \rightarrow 0$ , the tails become increasingly heavier [1]–[3]. It is shown in the literature that S $\alpha$ S models simulate impulsive noise very well [2], [4], [5]. Practical impulsive noise is encountered in a few environments. In [5], a thorough analysis of ambient noise in shallow underwater scenarios is presented. The noise is impulsive with S $\alpha$ S models offering a good fit for  $\alpha$  in the range 1.6 to 1.9.

With the exception of the Gaussian and Cauchy cases, S $\alpha$ S distributions do not exist in closed form. One way to bypass this issue involves working with the characteristic function (cf)

which is the Fourier transform of a pdf. Fortunately, the cf of S $\alpha$ S random variables exists in closed form.

Digital communication schemes are conventionally analyzed at the baseband level. In this paper we analyze the statistical properties of the baseband signal derived from passband additive white S $\alpha$ S noise (AWS $\alpha$ SN) using the cf approach. The bivariate pdf of any complex noise sample, though S $\alpha$ S, is generally not isotropic. Further still, the noise components may or may not be independent. By tweaking certain physical parameters of the system, the baseband noise distribution takes on various symmetric star-shaped configurations. These shapes are a result of the heavy-tailed phenomenon associated with impulsive noise pdfs. The spread of any distribution is quantified by its *scale parameter*. We investigate the relationship between the baseband noise scale parameter, the noise impulsiveness, system parameters and the passband noise scale parameter. The work presented here provides a fundamental understanding of impulsive noise contaminating conventional communication systems and creates a platform leading to robust system design.

In Section-II we briefly discuss S $\alpha$ S variables and vectors, the AWS $\alpha$ SN channel and passband-to-baseband conversion. In Section-III we investigate the properties of complex baseband noise derived from passband AWS $\alpha$ SN. Finally, we wrap up our discussion by summarizing our work in Section-IV.

## II. NOTATION AND CONCEPTS

### A. Symmetric $\alpha$ -Stable Variables & Vectors

A stable random variable  $X$  is S $\alpha$ S if its pdf  $f_X(x)$  is symmetric about  $X = 0$ , i.e,  $f_X(x) = f_X(-x)$ . The cf of  $X$  is given by:

$$\Phi_X(\theta) = \int_{-\infty}^{+\infty} f_X(x) \exp(i\theta x) = \exp(-\delta^\alpha |\theta|^\alpha) \quad (1)$$

where  $\delta \in (0, +\infty)$  is the *scale parameter* of the distribution [1]–[3]. The expression in (1) is a real and even function of the frequency-domain variable  $\theta$ , i.e,  $\Phi_X(\theta) = \Phi_X(-\theta) = \Phi_X^*(\theta)$ . In accordance to Fourier transform properties, this implies a real and symmetric pdf, i.e,  $f_X(x) = f_X(-x) = f_X^*(x)$ . The pdf of an S $\alpha$ S random variable is completely parameterized by  $\alpha$  and  $\delta$ . We therefore denote it using the abridged notation  $\mathcal{S}(\alpha, \delta)$ . For the Gaussian case,  $\mathcal{S}(2, \delta)$  is equivalent to  $\mathcal{N}(0, 2\delta^2)$ .

With the exception of the Gaussian case, all S $\alpha$ S distributions have algebraic tails. For  $0 < \alpha < 2$ ,

$$f_X(x) \sim \left( \frac{\alpha \delta^\alpha \sin(\pi\alpha/2) \Gamma(\alpha)}{\pi} \right) |x|^{-\alpha-1} \quad (2)$$

as  $|x| \rightarrow +\infty$  [1]. Here,  $\Gamma(\cdot)$  denotes the gamma function. From (2), it is observed that second order moments of non-Gaussian S $\alpha$ S distributions are infinite. Further still, for  $\alpha < 1$  even the first order moment is infinite.

For the multivariate case, the distribution  $f_{\vec{X}}(\vec{x})$  of a stable random *vector*  $\vec{X}$  is S $\alpha$ S if  $f_{\vec{X}}(\vec{x}) = f_{\vec{X}}(-\vec{x})$ . The cf is then real and symmetric about the frequency-domain *vector*  $\vec{\theta} = 0$ , i.e.,  $\Phi_{\vec{X}}(\vec{\theta}) = \Phi_{\vec{X}}(-\vec{\theta}) = \Phi_{\vec{X}}^*(\vec{\theta})$ . This relationship between a pdf and its cf is unique to symmetric distributions and is an appropriate test to validate if a stable distribution is indeed S $\alpha$ S or not [3].

Contrary to the univariate case, closed form cfs generally do not exist for multivariate S $\alpha$ S distributions. If an S $\alpha$ S random vector can be factored into  $\vec{X} \sim A^{1/2} \vec{G}$ , where  $\vec{G}$  is a zero-mean Gaussian vector and  $A$  is a totally right-skewed stable random variable independent of  $\vec{G}$ , then  $\vec{X}$  is  $\alpha$ -sub-Gaussian. Fortunately, the cf of  $\vec{X}$  then exists in closed form:

$$\Phi_{\vec{X}}(\vec{\theta}) = \exp \left( - \left| \frac{1}{2} \vec{\theta}^t \mathbf{R} \vec{\theta} \right|^{\alpha/2} \right) \quad (3)$$

where  $\mathbf{R}$  is the covariance matrix of  $\vec{G}$ . For the univariate case, an S $\alpha$ S distribution is  $\alpha$ -sub-Gaussian. This is observed by comparing (3) for scalar  $\vec{X}$  to (1). Multivariate S $\alpha$ S distributions, however, may not be  $\alpha$ -sub-Gaussian.

### B. The AWS $\alpha$ SN Channel

The AWS $\alpha$ SN model has been used in [4]–[7] to model impulsive noise with IID samples. We summarize the characteristics of AWS $\alpha$ SN below:

- All noise samples are IID with distribution  $\mathcal{S}(\alpha, \delta_p)$ .
- The joint-cf of any number of AWS $\alpha$ SN samples corresponds to the multiplication of their individual cfs.
- For  $\alpha = 2$ , AWS $\alpha$ SN reduces to the well-known additive white Gaussian noise (AWGN) process.
- Concepts of autocorrelation and power spectral density (PSD) do not directly extend to non-Gaussian AWS $\alpha$ SN as second order moments of stable distributions generally do not exist.
- The term ‘white’ simply signifies IID noise samples. It does not imply a flat PSD, as in the Gaussian case.

### C. Conversion to Baseband

The relationship between a discrete passband signal  $N[n]$  and its complex upsampled baseband form  $Z[n]$  is given by

$$N[n] = \Re \left\{ Z[n] \exp \left[ i 2\pi \frac{f_c}{f_s} n \right] \right\} \quad (4)$$

where  $f_s$  and  $f_c$  are the passband sampling and carrier frequencies, respectively [7], [8]. By convention, we reserve square brackets for discrete-time signals and parentheses for

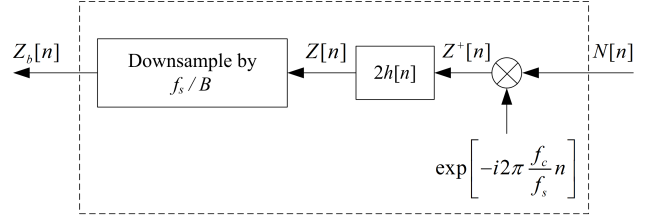


Fig. 1. A typical passband-to-baseband conversion system.

continuous-time signals. The relationship between a discrete signal and its continuous counterpart is of the form  $x[n] = x(n/f)$ , where  $n$  is the discrete-time index and  $f$  is the sampling frequency.

The schematic in Fig. 1 depicts the passband-to-baseband conversion process. In conventional passband-to-baseband conversion,  $N[n]$  is shifted by  $f_c/f_s$  in the spectral domain to get  $Z^+[n]$ . This is accomplished by multiplying  $N[n]$  with  $\exp[-i2\pi f_c/f_s n]$ . The result is then passed through a lowpass filter to get  $Z[n]$ . The filter is assumed to be of order  $M$  and cutoff  $\frac{B}{2f_s}$ , where  $B$  is the message symbol rate. Finally,  $Z[n]$  is downsampled by  $f_s/B$  to generate the baseband signal  $Z_b[n]$ , i.e.,  $Z_b[n] = Z[f_s/Bn]$ . For the remainder of this paper we assume the impulse response of the lowpass filter to be

$$h[n] = \begin{cases} \frac{B}{f_s} \text{sinc} \left[ \frac{B}{f_s} \left( n - \frac{M}{2} \right) \right] & \text{for } 0 \leq n \leq M \\ 0 & \text{otherwise} \end{cases} \quad (5)$$

where  $\text{sinc}$  is the *normalized sinc* function. A scale factor of 2 is incorporated in Fig. 1 so that (4) is satisfied. The Nyquist criterion is assumed to have been met, i.e.,  $f_s > 2f_c + B$ .

### III. COMPLEX BASEBAND S $\alpha$ S NOISE

The baseband signal  $Z_b[n]$  demonstrates interesting statistical behavior when  $N[n]$  are samples of an AWS $\alpha$ SN process. Using the passband-to-baseband conversion model in Fig. 1, the joint-cf of any complex sample  $Z[n]$  is given by [7]:

$$\Phi_{Z[n]}(\vec{\theta}) = \exp \left( - \sum_{k=0}^M \left| 2h^2(k) \vec{\theta}^t \mathbf{R} [n-k] \vec{\theta} \right|^{\frac{\alpha}{2}} \right) \quad (6)$$

where

$$\mathbf{R}[n] = 2\delta_p^2 \begin{bmatrix} \cos^2[2\pi \frac{f_c}{f_s} n] & -\frac{1}{2} \sin[4\pi \frac{f_c}{f_s} n] \\ -\frac{1}{2} \sin[4\pi \frac{f_c}{f_s} n] & \sin^2[2\pi \frac{f_c}{f_s} n] \end{bmatrix} \quad (7)$$

The objective of this paper is to analyze characteristics of baseband noise derived from non-Gaussian passband AWS $\alpha$ SN. Instead of presenting a rigorous proof, we offer an intuitive explanation of the noise pdf corresponding to (6). The statistical properties of  $Z_b[n]$  depend on the system parameters and passband noise statistics.

#### A. Independence of Time-Samples

From Fig. 1, the convolution operation in conjunction with the downsampling block allows each  $Z_b[n]$  to be expressed as a projection of  $Z^+[k]$  over  $\phi_n[k] = 2h[f_s n/B - k]$ . The

set of  $\phi_n[k] \forall n \in \mathbb{Z}$  are orthogonal vectors over  $k \in \mathbb{Z}$ . The orthogonal mapping and mutual independence of  $Z^+[n]$  ensures all  $Z_b[n]$  are independent for the Gaussian case. However, this result does not extend to other non-Gaussian AWS $\alpha$ SN scenarios. By setting  $M+1 \leq f_s/B$ , one ensures no overlap within the orthogonal function set, thus guaranteeing mutual independence of all  $Z_b[n]$ .

### B. Time-Invariance

We rewrite the joint-cf in (6) as

$$\Phi_{\vec{Z}[n]}(\vec{\theta}) = \exp(-p[n] * q[n]) \quad (8)$$

where

$$p[n] = |2h^2[n]|^{\alpha/2} \quad (9)$$

$$q[n] = |\vec{\theta}^T \mathbf{R}[n] \vec{\theta}|^{\alpha/2} \quad (10)$$

and  $*$  denotes the discrete-time linear convolution operation. To analyze the effect of the convolution term in (8), we look at  $p[n]$  and  $q[n]$  in the spectral domain.

In Fig. 2 we present the spectrum of  $p[n]$  for various values of  $\alpha$  with  $B = 1$ ,  $f_s = 21$  and  $M = 800$ . It is observed that  $p[n]$  is in essence a lowpass filter as it assigns frequencies near zero a larger weight in comparison to those further away. Further still, it assigns the largest weight to the dc component.

For  $q[n]$ , we expand (10) to get

$$q[n] = (2\delta_p^2)^{\alpha/2} \left| \theta_1^2 \cos^2 \left[ 2\pi \frac{f_c}{f_s} n \right] + \theta_2^2 \sin^2 \left[ 2\pi \frac{f_c}{f_s} n \right] - \theta_1 \theta_2 \sin \left[ 4\pi \frac{f_c}{f_s} n \right] \right|^{\alpha/2} \quad (11)$$

where  $\vec{\theta} = [\theta_1 \ \theta_2]^T$ . We note that  $q[n]$  is a periodic signal with period  $N = f_s/\text{gcd}(4f_c, f_s)$ , where  $\text{gcd}$  is the *greatest common divisor*. Irrespective of any  $\alpha$  and non-zero  $\theta$ ,  $q[n]$  may be broken into an exact sum of  $N$  equally-spaced, weighted harmonics. To support this argument we present the spectrum of an instance of  $q[n]$  with  $f_c = 4$ ,  $f_s = 21$  and  $\alpha = 1$  in Fig. 3. The spectrum has  $N = 21$  impulses, signifying each of the  $N$  harmonics.

According to Fourier transform properties, convolution in time implies multiplication in frequency domain [8]. The spectrum of the convolution term in (8) is then evaluated by multiplying the individual spectrums of  $p[n]$  and  $q[n]$ . The lowpass filtering effect of  $p[n]$  effectively nullifies all harmonics of  $q[n]$  with respect to the dc component. Thus  $p[n] * q[n]$  results in a constant-valued output. The joint-cf in (6) is thus time-invariant. Hence  $\Phi_{\vec{Z}_b[n]} = \Phi_{\vec{Z}[f_s n/B]} = \Phi_{\vec{Z}[n]}$ . For the Gaussian ( $\alpha = 2$ ) case, it is well known that baseband noise is time-invariant [8]. This property thus extends to all non-Gaussian ( $\alpha \neq 2$ ) AWS $\alpha$ SN cases.

### C. Star-Like Contour Structures

We gain insight into the pdf structure of each  $Z_b[n]$  by analyzing the distributions at various stages of the model in Fig. 1. Our observations are listed below:

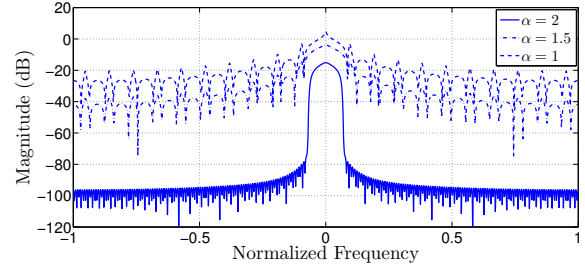


Fig. 2. Spectrum of  $p[n]$  for various values of  $\alpha$ .

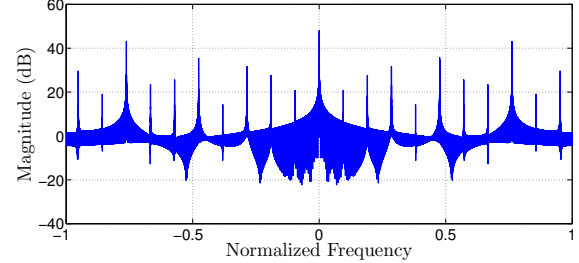


Fig. 3. Spectrum of  $q[n]$  for  $\alpha = 1$ .

- The pdf of each complex sample  $Z^+[n]$  is bivariate  $\alpha$ -sub-Gaussian. The distributions are degenerate and lie at an angle of  $-2\pi f_c/f_s n$  radians from the positive real axis in the complex plane.
- The linear convolution operation of the lowpass filter scales and multiplies  $M$  adjacent samples of  $Z^+[n]$ . As all  $Z^+[n]$  are mutually independent, the distribution of  $Z[n]$  stems from a two-dimensional convolution operation of  $M$  degenerate bivariate pdfs each lying at  $-2\pi f_c/f_s n$  radians from the positive real axis. As each  $Z^+[n]$  is heavy-tailed, one expects the distribution of  $Z[n]$  to consist of ‘tails’ along certain angles giving it a star-like structure. These tails are uniformly distributed about the origin and are determined by

$$\frac{f_s}{\text{gcd}(f_c, f_s)} \text{ if } f_s \text{ is an even multiple of } f_c \quad (12)$$

$$\frac{2f_s}{\text{gcd}(f_c, f_s)} \text{ otherwise}$$

- As  $Z_b[n] = Z[f_s/Bn]$ , the distribution of  $Z_b[n]$  is the same as  $Z[n]$  due to the previously established time-invariance property.

In Fig. 4 we present the bivariate pdf of  $Z_b[n]$  for the Cauchy case with parameters summarized in Table-I. As the Cauchy distribution exhibits the heavy-tailed phenomenon common to all non-Gaussian stable distributions, the star-like structures are observed in all non-Gaussian AWS $\alpha$ SN cases.

As the cf in (6) is real and an even function of  $\theta$ , each noise sample  $Z[n]$  and hence  $Z_b[n]$  is bivariate  $\mathcal{S}\alpha\mathcal{S}$ . With the exception of the Gaussian case, the components of any baseband sample may or may not be independent and the corresponding bivariate pdf is generally not isotropic. Further still, independent components do not imply isotropic distributions. From Fig. 4, one can see that as the number of tails tends to

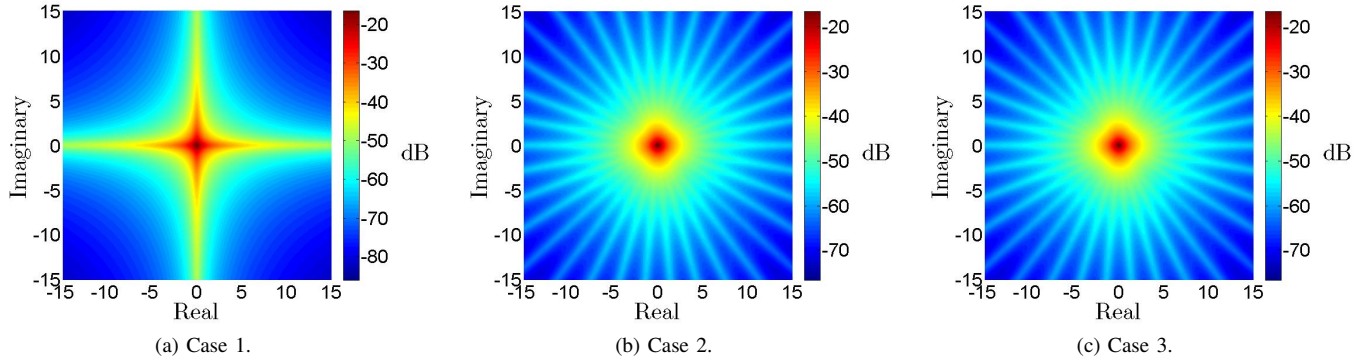


Fig. 4. Bivariate pdfs of  $Z_b[n]$  are presented for the Cauchy case ( $\alpha = 1$ ) under the assumption of passband AWS $\alpha$ SN. The parameters that generate each of these plots are summarized in Table-I.

TABLE I  
PARAMETER SETTINGS FOR GENERATING THE SCATTER PLOTS IN FIG. 4.

Case	$f_c$	$f_s$	Number of Tails	$B$	$\delta_b$
1.	4	16	4	1	1
2.	4	17	34	1	1
3.	4	24	6	1	1

infinity, the pdf converges to an isotropic distribution.

#### D. Marginal Distributions

Denoting the real and imaginary components of  $Z_b[n]$  by  $Z_R[n]$  and  $Z_I[n]$ , respectively, the marginal cfs of (6) are

$$\Phi_{Z_R[n]}(\theta) = \exp\left(- (2\delta_p)^\alpha \sum_{k=0}^M \left| h[k] \cos\left[2\pi \frac{f_c}{f_s}(n-k)\right] \right|^\alpha \theta^\alpha\right) \quad (13)$$

$$\Phi_{Z_I[n]}(\theta) = \exp\left(- (2\delta_p)^\alpha \sum_{k=0}^M \left| h[k] \sin\left[2\pi \frac{f_c}{f_s}(n-k)\right] \right|^\alpha \theta^\alpha\right) \quad (14)$$

On comparing (1), (13) and (14) we note that  $Z_R[n]$  and  $Z_I[n]$  are both univariate S $\alpha$ S. The marginal distributions of  $Z_b[n]$  are identical if the tails in the corresponding joint-pdf lie along both real and imaginary axes, as in Fig. 4a [7]. Also,  $Z_R[n]$  and  $Z_I[n]$  are almost identical if the number of tails is large. We may ensure identical components for all possible pdf configurations by slightly changing the expression in (4) to  $N[n] = \Re\left\{ Z[n] \exp\left(i\left(2\pi \frac{f_c}{f_s} n - \frac{\pi}{4}\right)\right)\right\}$ . We will however stick to (4) in accordance to convention.

#### E. The Case of Independent Components

For  $\alpha \neq 2$ , the real and imaginary components of  $Z_b[n]$  are independent if and only if  $f_s = 4f_c$ . This follows from the fact that (7) simplifies to a diagonal matrix thus allowing (6) to be decomposed into a product of its marginals. From (12), the pdf structure of  $Z_b[n]$  will then always have four tails. The

converse also holds, i.e., the four-tailed pdf corresponds to the case of independent components.

#### F. The Scale Parameter Relationship Equation

An important relationship is that of the baseband scale parameter with the noise impulsiveness and system parameters. As the marginal distributions are not exactly identical we restrict our analysis to the scale parameter in (13). We adopt a limiting approach that is also applicable to (14).

From (13) and (1), we have

$$\delta_b^\alpha = (2\delta_p)^\alpha \left( \sum_{k=0}^M \left| h[k] \cos\left[2\pi \frac{f_c}{f_s}(n-k)\right] \right|^\alpha \right) \quad (15)$$

where  $\delta_b$  is the scale parameter in (13). We note that  $\delta_b$  changes linearly with  $\delta_p$ . We comment on (15) for two special cases:

##### 1) The Gaussian Case:

For  $\alpha = 2$ , (15) reduces to

$$\delta_b^2 = (2\delta_p)^2 \frac{B}{f_s} \quad (16)$$

Thus  $\delta_b \propto \sqrt{B/f_s}$ . If  $N_0/2$  is the two-sided PSD of the AWGN process, then each sample of the passband noise process is  $\mathcal{N}(0, f_s N_0/2)$ . We may rewrite (16) as the well-known expression:

$$\delta_b^2 = \frac{BN_0}{2} \quad (17)$$

Thus each baseband noise sample is drawn from  $\mathcal{N}(0, BN_0)$ .

##### 2) Extremely Impulsive Noise:

As  $\alpha \rightarrow 0$ , the passband noise becomes increasingly impulsive. In the limit, (15) converges to

$$\delta_b^\alpha \rightarrow M + 1 \quad (18)$$

From (18), we note that  $\delta_b \propto (M + 1)^{1/\alpha}$ . The order of the FIR filter thus plays an important role in evaluating  $\delta_b$  as  $\alpha \rightarrow 0$ .

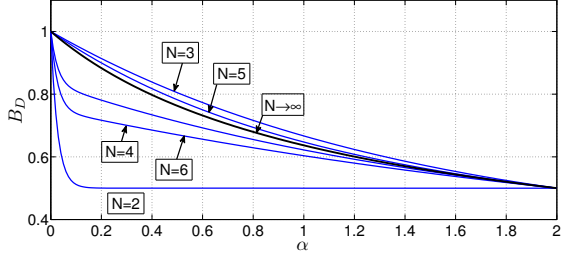


Fig. 5.  $B_D$  against  $\alpha$  for different values of  $N$ .

We will now analyze  $\delta_b^\alpha$  for the general S $\alpha$ S case. Eq. (15) may be written as

$$\delta_b^\alpha = (2\delta_p)^\alpha (a[n] * b[n]) \quad (19)$$

where

$$a[n] = |h[n]|^\alpha, \quad (20)$$

$$b[n] = \left| \cos \left( 2\pi \frac{f_c}{f_s} n \right) \right|^\alpha \quad (21)$$

As the joint-cf in (6) is time invariant, (19) simplifies to:

$$\delta_b^\alpha = (2\delta_p)^\alpha (A_D B_D) \quad (22)$$

where  $A_D$  and  $B_D$  are the dc terms of  $a[n]$  and  $b[n]$ , respectively. Noting that  $b[n]$  is periodic, we have from the Fourier transform

$$B_D = \frac{1}{N} \sum_{n=0}^{N-1} b[n] \quad (23)$$

where  $N = f_s / \text{gcd}(2f_c, f_s)$  is the period of  $b[n]$ . As  $N \rightarrow \infty$ ,  $B_D$  converges to

$$\begin{aligned} B_D &= \frac{f_s}{N} \sum_{n=0}^{N-1} b[n] / f_s = \frac{f_s}{N} \sum_{n=0}^{N-1} b(n/f_s) / f_s \\ &\rightarrow \frac{f_s}{N} \int_0^{\frac{N}{f_s}} b(t) dt \end{aligned} \quad (24)$$

Using the inherent structure of  $b(t)$ , (24) simplifies to

$$\begin{aligned} B_D &= 4f_c \int_0^{\frac{1}{4f_c}} b(t) dt \\ &= \frac{\Gamma\left(\frac{1+\alpha}{2}\right)}{\sqrt{\pi}\Gamma\left(1+\frac{\alpha}{2}\right)} \end{aligned} \quad (25)$$

Although (25) is evaluated for the limit  $N \rightarrow \infty$ , it offers a good approximation for a large range of  $N$ . In Fig. 5, we highlight this by plotting (25) and (23) against  $\alpha$  for increasing values of  $N$ . In the limit,  $B_D$  depends only on the impulsiveness, which is quantified by  $\alpha$ , and not on any of the system parameters  $B$ ,  $f_c$ ,  $f_s$  and  $M$ .

We note that (25) also extends to its counterpart in (14), i.e., if

$$b[n] = \left| \sin \left( 2\pi \frac{f_c}{f_s} n \right) \right|^\alpha \quad (26)$$

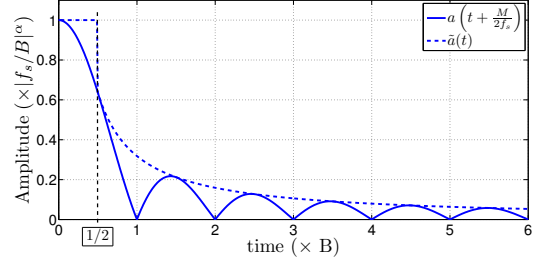


Fig. 6.  $a\left(t + \frac{M}{2f_s}\right)$  and  $\tilde{a}(t)$  against time for  $\alpha = 1$ .

then (25) is true as  $N \rightarrow \infty$ .

We will now focus on evaluating an analytical expression for  $A_D$ . From Fourier transform properties:

$$A_D = \sum_{k=0}^M a[k] \quad (27)$$

Using the same sequence of steps in (24) and noting that  $a(t)$  is symmetric about  $t = \frac{M}{2f_s}$ ,

$$\begin{aligned} A_D &\rightarrow f_s \int_0^{\frac{M+1}{f_s}} a(t) dt = 2f_s \int_{\frac{M}{2f_s}}^{\frac{2M+1}{2f_s}} a(t) dt \\ &= 2f_s \int_0^{\frac{M+1}{2f_s}} a\left(t + \frac{M}{2f_s}\right) dt \end{aligned} \quad (28)$$

As  $f_s \gg B$ , (28) is a good approximation for  $A_D$ . Evaluating (28) is still not trivial. We accomplish this by introducing a tight upper-bound  $\tilde{a}(t)$  for  $a(t + M/(2f_s))$ ,

$$\tilde{a}(t) = \begin{cases} \left| \frac{B}{f_s} \right|^\alpha & 0 \leq t < \frac{1}{2B} \\ \left| \frac{1}{\pi f_s t} \right|^\alpha & \frac{1}{2B} \leq t < \frac{M+1}{2f_s} \\ 0 & \text{elsewhere} \end{cases} \quad (29)$$

In Fig. 6, we compare both  $a(t + M/(2f_s))$  and  $\tilde{a}(t)$  for  $\alpha = 1$ . We observe that  $\tilde{a}(t)$  correctly highlights the decay in  $a(t + M/(2f_s))$  as  $t \rightarrow (M+1)/f_s$ . The bound becomes tighter as  $\alpha \rightarrow 0$ . On substituting  $a(t + M/(2f_s))$  by  $\tilde{a}(t)$  in (28) and solving, we get the following upper bound on  $A_D$ :

$$\begin{aligned} \tilde{A}_D &= \left( \frac{B}{f_s} \right)^{\alpha-1} \left( 1 + \frac{2^\alpha}{\pi^\alpha (\alpha-1)} \right) \\ &\quad - \left( \frac{1}{M+1} \right)^{\alpha-1} \left( \frac{2^\alpha}{(\alpha-1)\pi^\alpha} \right) \end{aligned} \quad (30)$$

To ensure adequate lowpass filtering in the passband-to-baseband conversion process,  $M$  has to be large enough. In practice, there is a limit to how large  $M$  can be as it adds to the complexity of the system. We may factor  $M+1$  into

$$M+1 = \frac{2f_s}{B} L \quad (31)$$

where  $L$  is a measure of the number of lobes of the sinc function in  $h[n]$ . For  $L = 1$ ,  $h[n]$  consists of only the main lobe. For  $L = 2$ , the main lobe and its two adjacent side lobes (one on either side) constitute  $h[n]$ . Usually  $L > 1$  to ensure

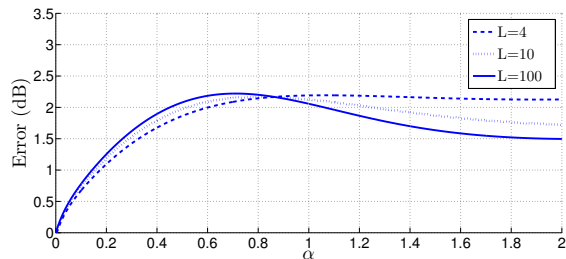


Fig. 7. Error (dB) between  $A_D$  and  $\tilde{A}_D$  against  $\alpha$ .

good lowpass filtering. In Fig. 7, we plot the error between  $\tilde{A}_D$  and  $A_D$  against  $\alpha$  for various values of  $L$  with  $B/f_s = 0.05$ . The error curve is almost the same for any  $f_s \gg B$ . Also, increasing  $L$  further hardly results in any difference. This shows that (30) tracks the transitions in  $A_D$  consistently for all possible combinations of the system parameters.

The bound in (30) is a fruitful result. For any given  $\alpha$ ,  $\tilde{A}_D$  is a function of  $1/(M+1)^{\alpha-1}$  and  $(B/f_s)^{\alpha-1}$ . As (30) is a tight bound, the trends observed in  $\tilde{A}_D$  against the system parameters can be extended  $A_D$ . We analyze these trends for three different cases:

- 1) *Gaussian-Like*: If  $M$  is large enough to guarantee adequate lowpass filtering, increasing  $M$  any further will not affect  $A_D$  significantly. For this case,  $B/f_s$  plays a larger role in determining  $\delta_b$ . From (17), it is known that  $M$  plays no part in the evaluation of the baseband noise spread for the Gaussian case. We may substitute (31) in (30) to get

$$A_D < c_{\alpha,L} \left( \frac{B}{f_s} \right)^{\alpha-1} \quad (32)$$

where

$$c_{\alpha,L} = 1 + \frac{2^\alpha}{(\alpha-1)\pi^\alpha} \left( 1 - \frac{1}{(2L)^{\alpha-1}} \right)$$

For  $\alpha$  within the vicinity of 2,  $c_{\alpha,L}$  is hardly affected by increasing  $L$  or  $\alpha$  and is almost constant.

- 2) *Cauchy-Like*: For the special case of  $\alpha = 1$ , (30) is

$$A_D < 1 + \frac{2 \ln(\frac{B}{f_s}) + 2 \ln(M+1)}{\pi} \quad (33)$$

It is observed that  $\tilde{A}_D$  increases logarithmically with  $B/f_s$  and  $M$ . Using (31), we may simplify this further to

$$A_D < 1 + \frac{2 \ln(2) + 2 \ln(L)}{\pi} \quad (34)$$

Thus  $\tilde{A}_D$  may be expressed solely as a function of  $L$ .

- 3) *Very Impulsive Noise*: As  $\alpha \rightarrow 0$ , the order  $M$  plays a more significant role than  $B/f_s$  in evaluating  $\delta_b$ . This can be seen from (18). Further still, as  $\alpha \rightarrow 0$ , (30) converges to (27). We may rewrite (30) as

$$A_D < d_{\alpha,L} (M+1)^{1-\alpha} \quad (35)$$

where

$$d_{\alpha,L} = \frac{1}{(2L)^{1-\alpha}} + \frac{2^\alpha}{(1-\alpha)\pi^\alpha} \left( 1 - \frac{1}{(2L)^{1-\alpha}} \right) \quad (36)$$

As  $\alpha \rightarrow 0$ ,  $d_{\alpha,L}$  depends less on  $L$  and  $\alpha$  and is almost constant.

On plugging (30) and (25) in (22) we see a direct relationship between  $\delta_b$ ,  $\delta_p$ ,  $B/f_s$  and  $M$ . As  $\delta_b^\alpha \propto A_D$ , the results in (32), (34) and (35) for  $A_D$  are easily extended to  $\delta_b^\alpha$ .

Practical impulsive noise is usually approximated well by AWS $\alpha$ SN for  $\alpha$  in the range of 1.6 and 1.9. In this range,  $B/f_s$  plays a pivotal role in determining  $\delta_b$ , as depicted by (32). In the literature, various signal-to-noise ratio (SNR) measures have been introduced to analyze error performance of digital communication systems [7], [9]. These measures are inversely proportional to  $\delta_b^2$ . Thus for practical impulsive noise

$$\text{SNR}_{\text{measure}} \propto \left( \frac{f_s}{B} \right)^{\frac{2(\alpha-1)}{\alpha}} \quad (37)$$

Similarly, if the noise is more impulsive, we may use (33) or (35) to see how the SNR varies in impulsive noise scenarios.

#### IV. CONCLUSION

In this paper we have investigated the characteristics of baseband noise derived from passband AWS $\alpha$ SN. The baseband noise samples are identically S $\alpha$ S and have star-like distributions. The scale parameter of the baseband noise distribution has been promptly analyzed and is shown to be a function of the system parameters and noise impulsiveness. The work presented in this paper offers exciting new findings about impulsive noise in conventional digital communication systems and provides a platform for robust system design in such scenarios.

#### REFERENCES

- [1] J. P. Nolan, *Stable Distributions - Models for Heavy Tailed Data*. Boston: Birkhauser, 2012, in progress, Chapter 1 online at academic2.american.edu/~jpnolan.
- [2] C. L. Nikias and M. Shao, *Signal processing with Alpha-Stable Distributions and Applications*. New York: Chapman-Hall, 1996.
- [3] G. Samorodnitsky and M. S. Taqqu, *Stable Non-Gaussian Random Processes: Stochastic Models with Infinite Variance*. Chapman & Hall, 1994.
- [4] M. Chitre, J. Potter, and S.-H. Ong, "Viterbi decoding of convolutional codes in symmetric  $\alpha$ -stable noise," *Communications, IEEE Transactions on*, vol. 55, no. 12, pp. 2230–2233, dec. 2007.
- [5] —, "Optimal and near-optimal signal detection in snapping shrimp dominated ambient noise," *Oceanic Engineering, IEEE Journal of*, vol. 31, no. 2, pp. 497–503, april 2006.
- [6] —, "Underwater acoustic channel characterisation for medium-range shallow water communications," in *OCEANS '04. MTS/IEEE TECHNO-OCEAN '04*, vol. 1, nov. 2004, pp. 40–45 Vol.1.
- [7] A. Mahmood, M. Chitre, and M. A. Armand, "PSK communication with passband additive symmetric  $\alpha$ -stable noise," *Communications, IEEE Transactions on*, [to appear].
- [8] J. Proakis, *Digital Communications*, 4th ed. Boston: McGraw-Hill, Aug. 2000.
- [9] J. G. Gonzalez, "Robust techniques for wireless communications in non-gaussian environments," Ph.D. dissertation, University of Delaware, Newark, DE, USA, 1997.